Mécanique & Industries 9, 167–174 (2008)
www.mecanique-industries.org
© AFM, EDP Sciences 2008
DOI: 10.1051/meca:2008022

Mécanique & Industries

Modelling dynamic fracture of thin shells filled with fluid: a fully SPH model

Alain Combescure[1,a], Bertrand Maurel[1,2] and Serguei Potapov[2]

[1] LaMCoS UMR CNRS 5259 INSA Lyon, 18–20 allée des sciences, 69621 Villeurbanne, France
[2] Électricité de France, Direction des études et recherches, 1 avenue du Général de Gaulle, 92141 Clamart Cedex, France

Received 25 mai 2007, Accepted 24 janvier 2008

Abstract – This paper is devoted to the description of a new full MLS SPH modelisation of rupture of thin shell filled with fluid and the prediction on consecutive fluid loss though the fracture. The paper first presents an efficient and controlled model for elastoplastic rupture of thin shells by a single layer of SPH balls. The proposed model controls as well static and dynamic instabilities using two basic ingredients: additional stress points to control the hourglass like instabilities and extend the Monhagan viscosity control method to shear and bending components of the generalized efforts. The fluid is modeled using standard SPH fluid model. The interaction is modeled using pin-balls method which is very natural in this type of formulation. Application examples are presented.

Key words: SPH / fluid-structure interaction / thin shells / plasticity / rupture / pin balls

Résumé – Modéliser la rupture dynamique de coques minces remplies de fluides avec des SPH. Cet article décrit une nouvelle méthode numérique pour modéliser la rupture de coques minces remplies de fluide et les débits de fuite qui en résultent. Cette méthode est une méthode MLS SPH. L'article donne d'abord une formulation efficace de la rupture d'une structure mince représentée par une seule nappe de SPH. Le modèle proposé est robuste car il contrôle à la fois les instabilités statiques et dynamiques. Ce contrôle repose que deux techniques : des points de contrôles additionnels qui permettent d'éviter les instabilités de type « sablier » et un modèle de viscosité artificielle du type Monhagan pour contrôler les instabilités des déformations de flexion. L'intéraction fluide structure repose sur une technique de « pinn balls » très naturelle pour les formulations SPH. On présente également des exemples d'application.

Mots clés : SPH / interaction fluide-structure interaction / coques minces / plasticité / rupture / pin balls

Introduction

The computation of fluid leakage in case of impact is a rather difficult topic. One may use a purely Eulerian approach for fluid and structure. This type of method is efficient but often introduces artificial loss of energy due to the treatment of partially filled elements. The association with level set associated with X-FEM techniques is a good modern solution: nevertheless X-FEM may not be the most efficient tool for fast transient dynamics. A recent paper [1] has given a method to solve fast transients in explicit dynamics using a lumped mass matrix. This method has been recently extended and tested for fluid structure interaction problems [2]. The meshless methods are very promising for fragmentation and rupture predictions including fluid splash modeling. A number of papers have tackled this difficult problem: one can cite [3–7]. The method is used for fluid and was more recently developed for solids including failure [8]. A few applications have been done for fluid structure interaction and very few for the case of shell fluid interaction. The existing papers mainly use EFG methods which have the advantage of being a weak formulation but the drawback of being rather expensive in terms of CPU time. This paper is devoted to a strong formulation base on a consistent formulation using SPH for the fluid as well as for the shell formulation. The paper is divided in 3 parts: the first one contains the main ingredients of the shell SPH formulation. The second one contains the fluid structure interaction formulation which is based on a pin ball approach. The third one describes numerical examples, starting from an academic case for shells up to the more complex interaction problem.

[a] Corresponding author: alain.combescure@insa-lyon.fr

1 SPH modelisation for fluid and structure

The SPH models for fluids are described rapidly in this section. The extension to solid behavior is a natural idea, but it induces one main difficulty which shall be explained in the second sub-section. The method can then be generalized to shell behavior including plasticity and rupture. This is contained in 3rd sub-section.

1.1 SPH models for fluid

The SPH model is represented by a set of points which we shall denote particles. All fields are represented by this set of particles. The fields are interpolated in any point in space using interpolating functions. We shall now restrict the presentation to the computation only on particles. The most commonly used interpolation function ϕ at particle i is described by Equation (1) :

$$\phi_{ij} = V_i W\left(r_{ij}, h\right) = V_i \frac{1}{\pi h^3} \begin{cases} 0 \text{ if } \frac{r_{ij}}{h} > 2 \\ \frac{1}{4}\left(2 - \frac{r_{ij}}{h}\right)^3 \text{ if } 2 > \frac{r_{ij}}{h} > 1 \\ \frac{3}{2}\left(\frac{2}{3} - \left(\frac{r_{ij}}{h}\right)^2 + \frac{1}{2}\left(\frac{r_{ij}}{h}\right)^3\right) \\ \text{if } 1 > \frac{r_{ij}}{h} > 0 \end{cases} \tag{1}$$

in Equation (1) V_i is the volume affected to particle i, W the kernel function, r_{ij} is the distance between particle j and i, and h the kernel function radius which defines its support and should be larger than the mean distance between the particles. Using this interpolation function one can approximate the value of a function f (respectively of its gradient) for particle i:

$$\begin{cases} f_i \cong f\left(\underline{x}_i\right) = \sum_{j=1}^{N} f_j \phi_{ij} & \text{(2a)} \\ \nabla f_i \cong \nabla f\left(\underline{x}_i\right) = \sum_{j=1}^{N} \left(f_j - f_j\right) \nabla \phi_{ij} & \text{(2b)} \end{cases}$$

In Equation (2a) N is the number of particles in the neighborhood of particle i (i.e. at a distance less than $2h$ of point i)[1].

Using Equation (2a) one can write the strong form of continuity and momentum conservation laws:

$$\begin{cases} \left(\frac{\partial \rho}{\partial t}\right)_i = -\rho_i \operatorname{div}\left(v\right) = -\rho_i V_i \sum_{j=1}^{N} \left(v_i - v_j\right) \nabla \phi_{ij} \\ \left(\frac{\partial v}{\partial t}\right)_i = \frac{\operatorname{div}\left(\sigma\right)}{\rho} = \sum_{j=1}^{N} \rho_j \left(\frac{\sigma_i}{\rho_i^2} + \frac{\sigma_j}{\rho_j^2} + \Pi_{ij}\right) \nabla \phi_{ij} \end{cases} \tag{3}$$

In the momentum conservation equation Π_{ij} is an artificial viscosity term which is added to avoid numerical instability in case of strong shock waves. Using constitutive equation for fluid or for solid we get a unique formulation valid for both type of material. The time integration of these equations uses for instance the explicit Newmark algorithm and sufficiently small time steps respecting the Courant's stability permits to compute the transient position of all particles. The formulation is Lagrangian as the position of particles changing at each time steps as well as the distances between particles allowing very easy fragmentation. This type of algorithm is very efficient and rather simple to implement for fluid impact simulation with rather complex fluid state equations.

[1] NB: Equations (2b) is a symetrised expression proposed by Monaghan to ensure that the gradient of f is null if f is a constant function.

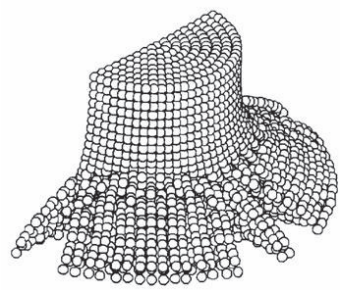

Fig. 1. Artificial uncontrolled fracture [9].

1.2 Solid

The solid formulation can be derived exactly in the same framework only changing the constitutive equation. It has been nevertheless observed that this updated Lagrangian formulation induces artificial fractures in the structures. Figure 1 displays the observed artificial uncontrolled fractures on a Taylor bar impact typical computation.

These artificial fractures have been shown [6] to come from numerical instabilities which can be controlled using a total Lagrangian formulation. The momentum Equation (3) then becomes:

$$\rho_i^0 \left(\frac{\partial v}{\partial t}\right)_i = \sum_{j=1}^{N} \left(\Pi_i + \Pi_j + \Pi_{ij}^0\right) \nabla^0 \phi_{ij}^0 \tag{4}$$

where ρ_i^0 is the initial density and π_i the transpose of the first Piola-Kirchoff stress tensor at particle i: the superscript 0 means that all quantities are evaluated on the initial geometry. A second instability cause is due to the nodal integration which leads to a sort of hourglass instability. This can be overcome using more points denoted "stress points" which are typically added at the barycentre of all possible tetraedra associated to the particles and where the stress are computed. Another problem comes from Equation (2a) which is a poor evaluation of the gradient. In order to improve accuracy moving least square interpolation functions are used. The final formulation called MLSPH method consists to replace the ϕ function by a more complex Φ function. This better approximation function is computed using a rather lengthy procedure which is explained for instance in Maurel [10].

1.3 Shell

The same ideas can be extended to Mindlin-Reissner shells. The SPH mesh is now a unique layer of particles which represent the mean surface of the shell. A thickness is attached to each mid plane particle; this thickness can of course change with time. Each particle has 5 degrees of freedom three translations and two rotations in the tangent plane to the shell. There is no drilling rotation. The MLS interpolation of the coordinates is used to define the geometries, as well as the tangent and normal vectors to the mean surface. The strong form of shell equilibrium equation is used. The global variable (resultant forces as well as shear forces and moments) are directly used for the equilibrium equations. These variables are linked to the membrane transverse shear and bending strains through the "global" stress strain law. Three different configurations are needed: the general fixed reference Cartesian configuration C_0, the local initial configuration denoted C_{L0} (defined by the initial normal and the two tangent initial vectors to the shell) and the actual local configuration denoted C (defined by the current normal and the two tangent vectors). Let us define the coordinates in this three configurations:

$$\begin{cases} \boldsymbol{x}_0 \text{ coordinates in configuration } C \\ \boldsymbol{x}_{L0} \text{ coordinates in configuration } C_{L0} \\ \boldsymbol{x}_L \text{ coordinates in configuration } C_L \end{cases} \tag{5}$$

The pseudo normal (which is the geometrical normal at the initial state, but which may be different when the shell is deformed) in the reference Cartesian configuration shall be denoted $\boldsymbol{n}\,(n_x, n_y, n_z)$. Let us now define the position $\boldsymbol{X}$ and the displacement $\boldsymbol{U}$ of a point M situated on the pseudo normal at a distance ξ from the mid plane:

$$\begin{cases} \boldsymbol{X}\,(\mathrm{M}) = \boldsymbol{X}^{\mathrm{m}} + \xi\,\boldsymbol{n} \\ \boldsymbol{U}\,(\mathrm{M}) = \boldsymbol{U}^{\mathrm{m}} + \xi \Delta \boldsymbol{n} = \boldsymbol{U}^{\mathrm{m}} + \xi\,(\boldsymbol{n} - \boldsymbol{n}_0) \end{cases} \tag{6}$$

In Equation (6) $\boldsymbol{n}_0$ is the initial normal vector. We can define two rotation matrices denoted G and R such that:

$$\begin{cases} \boldsymbol{x}_{L0} = G\boldsymbol{x}_0 \\ \boldsymbol{x}_L = R\boldsymbol{x}_0 \end{cases} \tag{7}$$

Let us now define the gradient matrix F as:

$$F = G \cdot F_3 \qquad \text{with} \quad F_3 = \begin{bmatrix} u_{x,x_{L0}} & u_{x,y_{L0}} & \Delta n_{x_{L0}} \\ u_{y,x_{L0}} & u_{y,y_{L0}} & \Delta n_{y_{L0}} \\ u_{z,x_{L0}} & u_{y,y_{L0}} & \Delta n_{z_{L0}} \end{bmatrix} \tag{8}$$

This expression of the gradient matrix allows to define the Green-Lagrange strain tensor which will have two parts. The first one E^{m} is constant across the thickness consisting of membrane and shear strains and the second one E^{b} is linear which is the bending strain:

$$\begin{cases} E_{hk}\,(\boldsymbol{X}) = \frac{1}{2}\left(U_{0h,k} + U_{0k,h} + \sum\limits_{l=1}^{3} \frac{\partial U_l}{\partial x_{0k}} \frac{\partial U_l}{\partial x_{0h}}\right) = E^{\mathrm{m}}_{hk} + E^{\mathrm{b}}_{hk} \\ E^{\mathrm{m}}_{hk} = \frac{1}{2}\left(U^{\mathrm{m}}_{0h,k} + U^{\mathrm{m}}_{0k,h} + \sum\limits_{l=1}^{3} \frac{\partial U^{\mathrm{m}}_l}{\partial x_{0k}} \frac{\partial U^{\mathrm{m}}_l}{\partial x_{0h}}\right) \\ E^{\mathrm{b}}_{hk} = \frac{\xi}{2}\left(\Delta n^{+}_{0h,k} \Delta n_{0k,h}\right) \end{cases} \tag{9}$$

These strains must then be rotated to the current local configuration to be able to write the plane stress-strain law and the shear stress strain law. The local strains are:

$$\begin{cases} \varepsilon^{\mathrm{m}}_L = R \cdot F^{-T} E^{\mathrm{m}} F^{-1} R^T \\ \varepsilon^{\mathrm{b}}_L = R \cdot F^{-T} E^{\mathrm{b}} F^{-1} R^T \end{cases} \tag{10}$$

Let us now define the vector representation of membrane shear and bending strains ε and stresses σ as:

$$\begin{cases} \boldsymbol{\varepsilon}^{\mathrm{m}}_g = \left(\varepsilon^{\mathrm{m}}_{Lxx}, \varepsilon^{\mathrm{m}}_{Lyy}, \varepsilon^{\mathrm{m}}_{Lxy}\right) \quad \boldsymbol{\sigma}^{\mathrm{m}}_g = \left(\sigma^{\mathrm{m}}_{Lxx}, \sigma^{\mathrm{m}}_{Lyy}, \sigma^{\mathrm{m}}_{Lxy}\right) \\ \boldsymbol{\varepsilon}^{\mathrm{s}}_g = \left(\varepsilon^{\mathrm{m}}_{Lxz}, \varepsilon^{\mathrm{m}}_{Lyz}, 0\right) \quad \boldsymbol{\sigma}^{\mathrm{s}}_g = \left(\sigma^{\mathrm{s}}_{Lxz}, \sigma^{\mathrm{s}}_{Lyz}, 0\right) \\ \boldsymbol{\varepsilon}^{\mathrm{b}}_g = \left(\varepsilon^{\mathrm{b}}_{Lxx}, \varepsilon^{\mathrm{b}}_{Lyy}, \varepsilon^{\mathrm{b}}_{Lxy}\right) \quad \boldsymbol{\sigma}^{\mathrm{b}}_g = \left(\sigma^{\mathrm{b}}_{Lxx}, \sigma^{\mathrm{b}}_{Lyy}, \sigma^{\mathrm{b}}_{Lxy}\right) \end{cases} \tag{11}$$

The usual stress strain laws link the stresses and strains for linear behavior:

$$\begin{cases} \boldsymbol{\sigma}^{\mathrm{m}}_g = C\boldsymbol{\varepsilon}^{\mathrm{m}}_g \\ \boldsymbol{\sigma}^{\mathrm{s}}_g = C'\boldsymbol{\varepsilon}^{\mathrm{s}}_g \\ \boldsymbol{\sigma}^{\mathrm{b}}_g = C\boldsymbol{\varepsilon}^{\mathrm{b}}_g \end{cases} \quad \text{where} \quad \begin{cases} C = \frac{E}{1-\nu^2} \begin{bmatrix} 1 & \nu & 0 \\ \nu & 1 & 0 \\ 0 & 0 & \frac{1-\nu}{2} \end{bmatrix} \\ C' = \frac{E}{2(1+\nu)} I \end{cases} \tag{12}$$

In the linear case the definition of resultants is:

$$\begin{cases} \boldsymbol{N} = h\boldsymbol{\sigma}^{\mathrm{m}}_g \\ \boldsymbol{T} = h\boldsymbol{\sigma}^{\mathrm{s}}_g \\ \boldsymbol{M} = \frac{h^3}{12}\boldsymbol{\sigma}^{\mathrm{b}}_g \end{cases} \tag{13}$$

We now introduce a matrix representation of these vectors:

$$\mathrm{S} = \begin{bmatrix} N_{xx} & N_{xy} & T_{xz} \\ N_{xy} & N_{yy} & T_{yz} \\ T_{xz} & T_{yz} & 0 \end{bmatrix} \quad \text{and} \quad \mathrm{M} = \begin{bmatrix} M_{xx} & M_{xy} & 0 \\ M_{xy} & M_{yy} & 0 \\ 0 & 0 & 0 \end{bmatrix} \tag{14}$$

The nominal membrane stress tensor can then be defined by:

$$P_0 = R^{\mathrm{T}} S R F^{\mathrm{T}} \tag{15}$$

The membrane and transverse shear equilibrium equation then writes in the reference configuration:

$$P_0^{\mathrm{T}} . \boldsymbol{\nabla}_0 = h\rho_0 \ddot{\boldsymbol{U}}_m \tag{16}$$

Let us define L, M_0 and $\boldsymbol{T}_0$ as:

$$L = \begin{bmatrix} 0 & 1 & 0 \\ 1 & 0 & 0 \\ 0 & 0 & 0 \end{bmatrix} \quad M_0 = JF^{-1}R^{\mathrm{T}} M L^{\mathrm{T}} R\, \boldsymbol{T}_0 = JR\boldsymbol{T} \tag{17}$$

where $J = \det\,(F)$

The bending equilibrium equation then writes in the reference configuration:

$$M_0^T . \boldsymbol{\nabla}_0 + \boldsymbol{T}_0 = I_0 \ddot{\boldsymbol{\theta}}_0 \tag{18}$$

where $\ddot{\boldsymbol{\theta}}_0$ and I_0 are respectively the rotation of the normal vector and the inertia. If we now introduce the ML-SPH interpolation functions one obtains:

$$\begin{cases} \rho_0 h \dot{\boldsymbol{V}}^i = \sum\limits_{j=1}^{N} P_j \boldsymbol{\nabla}_0 \Phi'_{0_{ij}} \\ I_0 \ddot{\boldsymbol{\theta}}^i_0 = \sum\limits_{j=1}^{N} M_j \boldsymbol{\nabla}_0 \Phi'_{0_{ij}} + \boldsymbol{T}_0 \end{cases} \quad \text{where } \Phi'_{0_{ij}} = G_{ik} . \Phi_{,x^i_{L0}} \tag{19}$$

The first line of Equation (19) defines the acceleration of the mean shell plane. The second one gives the angular acceleration of the pseudo normal vector. Let us now define the Q matrix which defines the rotation between the initial and the current position of the pseudo normal vector. The Newmark integration scheme is used to determine the increment of displacement of the mean surface as well as the increment of rotation matrix ΔQ. The update of the rotation matrix is computed with Rodriguez [11] formula:

$$\begin{cases} Q^{t+\Delta t} = \Delta Q.Q^t \\ \boldsymbol{n}^{t+\Delta t} = Q^{t+\Delta t}.\boldsymbol{n}_0 \end{cases} \tag{20}$$

The preceding equations are defining the procedure to compute movement of shells with SPH formulation in linear stress strain relations case. The present formulation is unstable for two reasons: the first one is the quality of the integration previously mentionned which induces hourglass type instability for shells as well as for solid cases. As for solid cases additional "stress" points are added at the barycentre of all elementary triangles of the particle mesh. In the equilibrium equations the neighbouring particles are repacled by the N_p stress points which belong to the influence zone of this node. Equations (19) then become:

$$\begin{cases} \rho_0 h \dot{\boldsymbol{V}}^i = \sum\limits_{p=1}^{N_p} P_p \boldsymbol{\nabla}_0 \Phi'_{0ip} \\ I_0 \ddot{\boldsymbol{\theta}}_0^i = \sum\limits_{p=1}^{N_p} M_p \boldsymbol{\nabla}_0 \Phi'_{0_{ip}} + \boldsymbol{T}_0 \end{cases} \tag{21}$$

Plasticity can be taken into account using Ilyushin [12] general plasticity model developed in Zeng [13]. This model is based on the simplified model of plastic hinges. The plastic yield function is given by the following equation

$$\begin{cases} (\sigma*)^2 - (\sigma_y(p))^2 = \left(\sigma_g^{\mathrm{m}^{\mathrm{eq}}}\right)^2 + \alpha^2 \left(\sigma_g^{\mathrm{b}^{\mathrm{eq}}}\right)^2 + \frac{\alpha}{\sqrt{3}} \sigma_g^{\mathrm{m}^{\mathrm{eq}}} \sigma_g^{\mathrm{b}^{\mathrm{eq}}} \\ \qquad + \kappa^2 \left(\sigma_g^{\mathrm{s}^{\mathrm{eq}}}\right)^2 - (\sigma_y(p))^2 \\ \left(\sigma_g^{\mathrm{m}^{\mathrm{eq}}}\right)^2 = \sigma_{g11}^{\mathrm{m}^2} + \sigma_{g22}^{\mathrm{m}^2} + 3\sigma_{g12}^{\mathrm{m}^2} - \sigma_{g11}^{\mathrm{m}} \sigma_{g22}^{\mathrm{m}} \\ \left(\sigma_g^{\mathrm{b}^{\mathrm{eq}}}\right)^2 = \sigma_{g11}^{\mathrm{b}^2} + \sigma_{g22}^{\mathrm{b}^2} + 3\sigma_{g12}^{\mathrm{b}^2} - \sigma_{g11}^{\mathrm{b}} \sigma_{g22}^{\mathrm{b}} \\ \left(\sigma_g^{\mathrm{s}^{\mathrm{eq}}}\right)^2 = 3\sigma_{g13}^{\mathrm{s}^2} + 3\sigma_{g23}^{\mathrm{s}^2} \\ \sigma_g^{\mathrm{m}^{\mathrm{eq}}} \sigma_g^{\mathrm{b}^{\mathrm{eq}}} = \sigma_{g11}^{\mathrm{m}} \sigma_{g11}^{\mathrm{b}} + \sigma_{g22}^{\mathrm{m}} \sigma_{g22}^{\mathrm{b}} + 3\sigma_{g12}^{\mathrm{m}} \sigma_{g12}^{\mathrm{b}} \\ \qquad - \frac{1}{2} \left(\sigma_{g11}^{\mathrm{m}} \sigma_{g22}^{\mathrm{b}} + \sigma_{g11}^{\mathrm{b}} \sigma_{g22}^{\mathrm{m}}\right) \end{cases} \tag{22}$$

In this equation the parameter α is chosen to be between 1 and 2/3 and the parameter κ will be given a null value for practical applications. The parameter α can be made a function of cumulated equivalent plastic strain to mimic the pseudo hardening to the progressive plastification of the section. This concept first developed by Crisfield is clearly explained in Zeng [14]. One may observe that in absence of bending and shear one has the standard plane stress plasticity model and this allows introducing directly the material hardening directly in the function $\sigma_y(p)$ where p is the cumulated equivalent plastic strain.

The normality rule and radial mapping return algorithm is used for the computation of plastic strains.

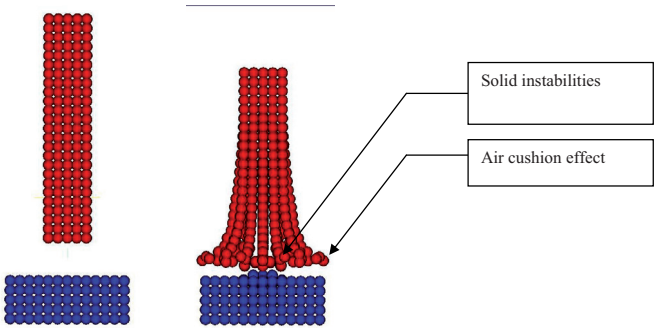

Fig. 2. Air cushion effect.

A crude failure criterion has been added simply based on the variation of distance between two particles. A link between to neighbor particles is broken if the separate too much. The following equation describes the failure criterion:

$$d_{ij} \geqslant (1 + \varepsilon_R)\, d_{0ij} \tag{23}$$

The failure "pseudo strain" ε_R is chosen to be 30% in the following.

2 Fluid structure interaction strategy

The fluid structure interaction is described in this section. Both medium are described using SPH formulations described in the previous section. The simplest implementation of a 2 media SPH is to give an attribute to each SPH particle assigning it to be either fluid or structure. This attribute allows specifying different types of interactions. Two modelisations of the interaction are possible.

2.1 Natural method

This method simply uses the influence radius of fluid on one side and of the structure on the other side to ensure the interaction which is then described as "natural". Nevertheless the interaction forces can be computed using either fluid or solid properties in the contact zone. The most simple interaction formula consist to take the interaction forces computed with fluid properties because they "naturally" take into account the unilateral nature of the contact: a fluid cannot stand negative pressures. This natural method is rather simple to implement but has two drawbacks: the first one is a poor representation of the normal to the surface and the second one is an artificial air cushion effect. The fluid never "touches" the solid, because the repulsion forces shall prevent the fluid to impact the structure: the thickness of the "air cushion" is the h radius of the interpolation function. Figure 2 illustrates this problem on an academic example.

2.2 Pin balls

An alternative method to model the fluid structure contact is to use the pin balls method as proposed by

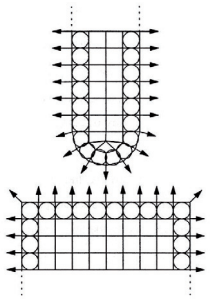

Fig. 3. 2D pin ball and normal definition.

Belytschko & Neal [14] and later developed in Europlexus software [15]. This method has the advantage of a precise definition of the normal to the interface as well as of the geometry of the boundary. The pin balls are laid on the external surfaces of the two impacting bodies and hence allow a precise definition of the direction of interaction forces. This method allows having a simple and efficient algorithm for contact detection. Figure 3 displays a simple view of the pin balls discretisation for a bi-dimensional situation.

The contact is searched using and extremely simple criterion described by the following equation:

$$d_{ij} \prec R_i + R_j \tag{24}$$

where d_{ij} is the distance between the two pin balls i and j and R_i, R_j the radius affected to each of them. This method is very efficient and simple but requires the definition of the radii of the pinball. Once the contact is detected contact forces are applied in the direction ij. The contact force can be computed using either a penalty method or Lagrange multiplier technique. The accelerations are first computed ignoring contact forces and are corrected in a second step in such a way that the contacts are respected. The correction of accelerations a_c^{n+1} at time step $n+1$ is given by the equation:

$$a_c^{n+1} = \mathrm{M}^{-1}\boldsymbol{\lambda}^{n+1} \tag{25}$$

where M is the mass matrix and λ^{n+1} the contact forces Lagrange multiplier at time step $n+1$. This vector is given by the following equation:

$$\begin{cases} \boldsymbol{\lambda}^{n+1} = \underline{\underline{B}}^{-1}.\bar{W} \\ \underline{\underline{B}} = \underline{\underline{C M^{-1} C^{\mathrm{T}}}} \\ \bar{W} = -\frac{2}{\Delta t^n + \Delta t^{n+1}} \underline{\underline{C}} \boldsymbol{V}^{n+1/2} \end{cases} \tag{26}$$

In Equation (26) $\underline{\underline{C}}$ is the constraint matrix associated with the active contacts $\boldsymbol{V}^{n+1/2}$ the mid step velocity vector. This equation ensures that the contact is active at time step $n+1$.

3 Numerical examples

This section contains numerical examples for shell computations as well as for fluid structure interactions.

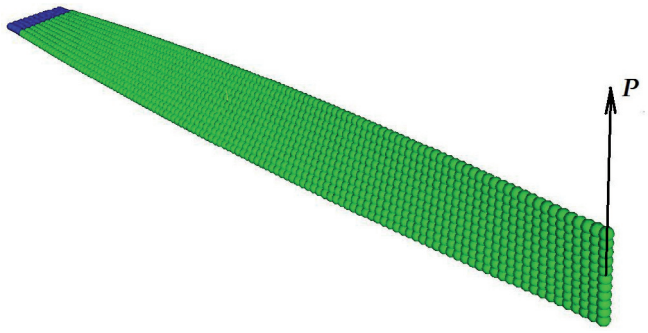

Fig. 4. Geometry of the twisted beam.

3.1 Shell examples

The first example is devoted to an academic case: the twisted beam example. The geometry is given in Mac Neal & Harder [16]. The mesh is displayed in Figure 4. Its length is 12 m, its thickness 0.032 m, width 1.1 m. The Young's modulus is 290 MPa, the Poisson's ratio 0.22 and the density 7800 kg.m^{-3}.

The computed results of the maximum vertical displacement of the extremity of the beam (0.1078 m) are in very good agreement with the reference value of 0.1084 m.

The second one is a complex non-linear shell problem which is rather well known in the literature and which illustrates the quality of the proposed method for geometrically non-linear problem. It is a pinched cylinder under very large displacements and rotations described by Jiang & Chernuka [9]. This cylinder has a radius of 4.953 m, a length of 10.35 m and a thickness of 0.094 m. The mesh and loading are displayed in Figure 5a. The Young's modulus is 1.05 MPa and the Poisson's ratio 0.3125. The final deformed shell is drawn in Figure 5b, and the load displacement is compared with the literature values in Figure 6. The predictions are good for this rather complex non-linear case.

The third example is an elastoplastic case. One takes a square plate of 1 m side and 0.01 m thickness clamped on its contour and submitted to pressure step of 16 MPa. The material has an elastic modulus of 200 000 MPa, a Poisson's ratio of 0.3 and a density of 7800 kg.m^{-3}. It is elastoplastic perfect plasticity. The yield stress is 400 MPa. The deformed shell is displayed in Figure 7 and the comparison with a finite-element analysis of the same problem using MITC4 elements with 5 points across the thickness is displayed in Figure 8.

The 4th one is a perforation case which illustrates the interest of the proposed rupture formulation. The same square plate as before is impacted by a rigid spherical mass of 2 kg and of 0.02 m diameter with an initial velocity of 300 m.s^{-1}. The perforated plate with two different meshes has always the same rupture pattern that is the same number of petals (here 8). Figure 9 displays the perforated plate. One may observe that there is no bending

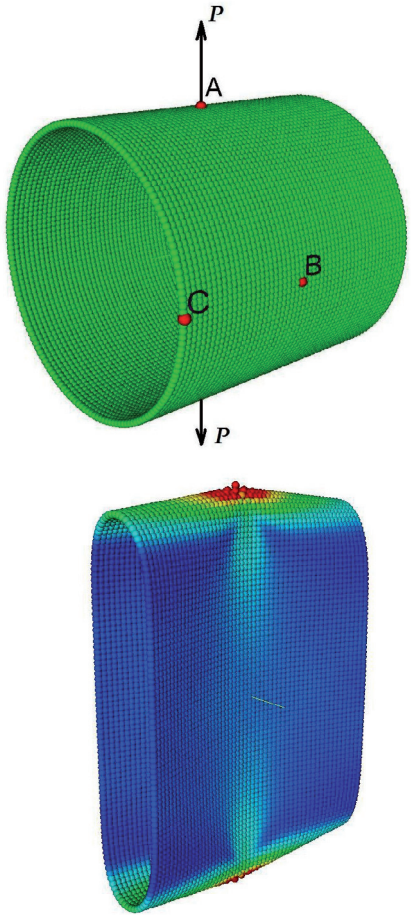

Fig. 5. a) Initial undeformed mesh, b) deformed pinched cylinder (amplification 1).

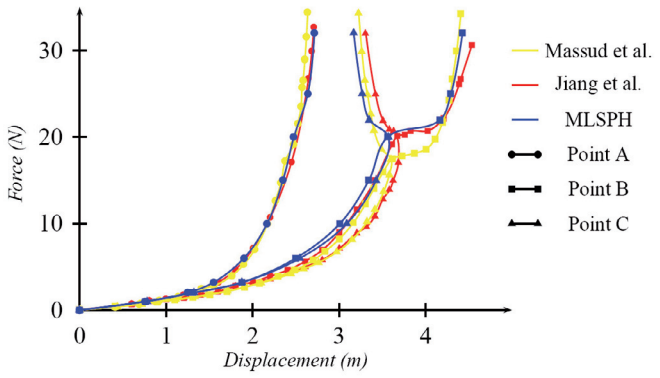

Fig. 6. Load displacement curve.

at the perforation time. This is due to the high energy of the impactor. The bending mode of the plate will occur later.

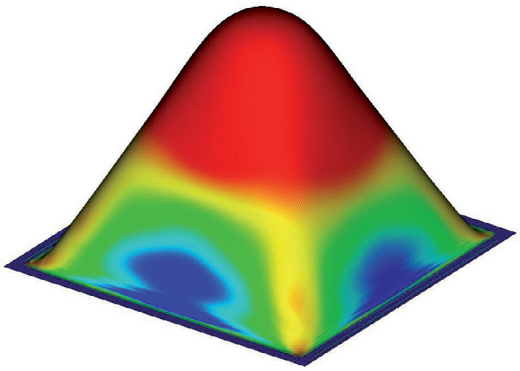

Fig. 7. Deformed SPH shell at maximum displacement.

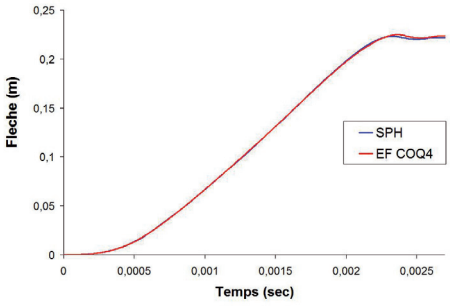

Fig. 8. Finite-element SPH comparison.

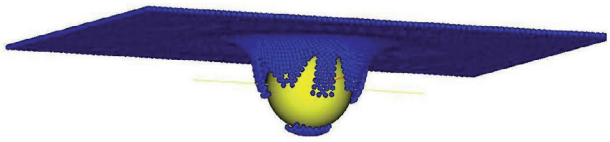

Fig. 9. Perforated plate: fine mesh.

3.2 Fluid structure interaction

In this section we shall show simple cases without perforation. The first example is devoted to the prediction of pressures and piston displacement in a shock tube ended by a plate mounted on a spring. The tube has a square section of 0.1 m side and initial water column length L_{F} of 1.0 m. The problem and its model are displayed in Figure 10. The SPH mesh is shown in Figure 11. The piston and its stiffness are modeled by a solid medium having the same square surface and a length L_{S} of 0.2 m. The fluid is water ($\rho_F = 1000$ kg.m^{-3}), and the solid has the following properties ($\rho_{\mathrm{S}} = 2000$ kg.m^{-3}, $E = 200\,000$ MPa, $\nu = 0.0$) where ρ_i is the specific mass of medium i, E the Young's modulus, ν the Poisson's ratio. We apply a constant longitudinal tension force $F = 12\,500$ N at the free end of the solid. This force is equally distributed to all solid particles lying on the fluid-structure interface.

The predicted displacement and pressure time histories are compared with reference finite-element and

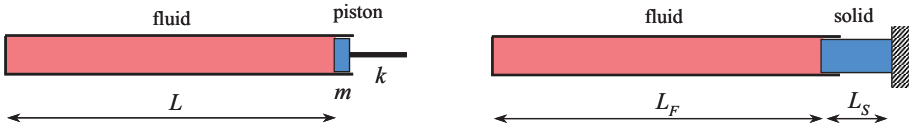

Fig. 10. Theoretical problem and its model.

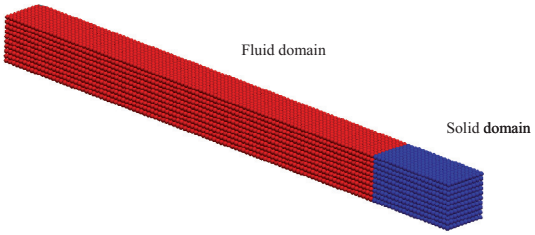

Fig. 11. SPH mesh.

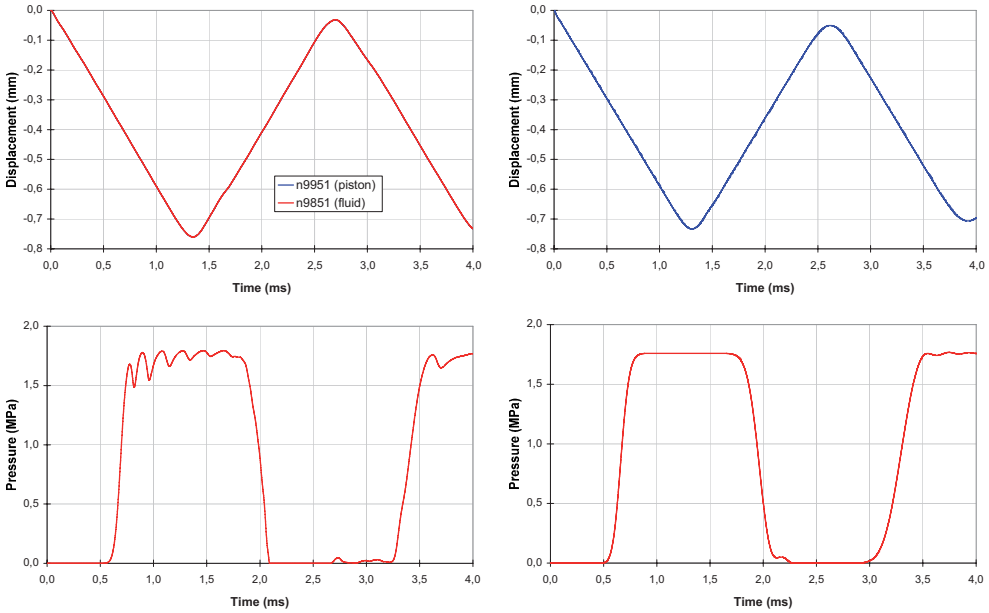

Fig. 12. FSI computation: SPH solution (left) and FE-FV solution (right).

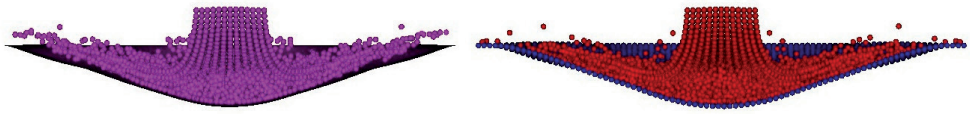

Fig. 13. Deformed fluid structure geometries (MITC4 shell (left) and SPH shell (right)).

finite-volume ones in Figure 12. The predictions are of good quality: the maximum displacement is 0.76 mm that means 1% error from the analytical solution. The SPH predicted first eigenfrequency of the coupled system, is found to be 2310 rad.s^{-1} and is very close (1.7% error) to the analytical value (2270 rad.s^{-1}).

The same square elastic plate as before is now impacted by a water column having a square basis of 5 cm and a height of 25 cm at an initial speed of 500 m.s^{-1}. The water column is meshed with fluid SPH and the plate is either meshed with MITC4 elements or with SPH shells. The deformed computed geometries of the fluid column as well as of the plate with the two shell modelisations are compared in Figure 13.

The evolution with time of the vertical displacement of the center of the plate is displayed in Figure 14. The agreement is rather good.

4 Conclusion and perspectives

This article describes a general method using only SPH formulation for fluid structure interaction in case of impact loadings. The proposed shell formulation gives rather interesting results. It includes non linear material response based on Ilyushin theory of plasticity as well a crude but efficient rupture criterion. The coupling procedure with fluid is also presented. Coupled simple analysis

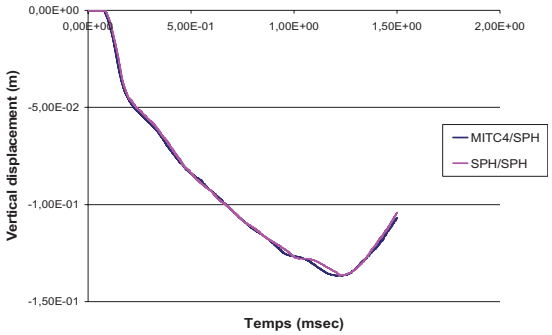

Fig. 14. Comparison of MITC4 and SPH shell plate models: vertical displacement of the center of the plate in case of fluid structure impact.

are presented and compared with other results from alternative methods or from the literature. This method shall be soon applied to fluid leakage predictions in case of impact loadings.

Acknowledgements. The support of EDF DER is gratefully acknowledged.

References

[1] T. Menouillard, R.J. Rethoré, A. Combescure, H. Bung, Efficient explicit time stepping for the extended finite element method (X-FEM), Int. J. Num. Meth. Eng. 68 (2006) 911–939

[2] A. Kolke, A. Legay, Enriched space time integration for fluid structure interaction: Part II, Thin flexible structures, Proc. 3rd European conference on computational mechanics, 5–6 June 2006, Lisbon

[3] R.A. Gingold, J.J. Monaghan, Smoothed particle hydrodynamics: theory and application to non-spherical stars, MNRAS 181 (1977) 375–382

[4] J.P. Gray, J. Monaghan, SPH elastic dynamics, Computer Meth. Appl. Mech. Eng. 190 (2001) 6641–6662

[5] T. Belytschko, Y. Guo, W.K. Liu, S.P. Xiao, A unified stability analysis of meshless particle methods, Int. J Num. Meth. Eng. 40 (2000) 1359–1400

[6] T. Belytschko, T. Rabczuk, S.P. Xiao, Stable particle methods based on Lagrangian kernels, Comp. Meth. Appl. Mech. Eng. 193 (2005) 1035–1063

[7] T. Rabczuk, P.M.A. Areias, T. Belytschko, A meshfree method for non-linear dynamic fracture, Int. J. Num. Meth. Eng., in press

[8] T. Rabczuk, T. Belytchko, Cracking particles: a simplified meshfree method for arbitrary evolving cracks, Int. J. Num. Meth. Eng. 61 (2004) 2316–2343

[9] Johnson, Beissel, SPH for high velocity impact computations, Comp. Meth. Appl. Mech. Eng. 139 (1996) 347–373

[10] B. Maurel, Modélisation numérique de la rupture de réservoirs remplis de fluide par la méthode SPH couplée fluide coque, Thèse INSA, Lyon, 24 janvier 2008

[11] P. Betsch, A. Menzel, E. Stein, On the parametrization of finite rotations in computational mechanics, Comp. Meth. Appl. Mech. Eng. 155 (1998) 273–305

[12] A.A. Ilyushin, Plasticité, Eyrolles, 1956

[13] Q. Zeng, A. Combescure, F. Arnaudeau, An efficient plasticity algorithm for shell elements application to metal forming simulations, Comp. Struct. 79 (2001) 1525–1540

[14] T. Belytschko, M.O. Neal, Contact-Impact by the Pinball method with penalty and Lagrangian Methods, Int. J. Num. Meth. Eng. 31 (1991) 547–572

[15] F. Casadei, A General Impact-Contact Algorithm based on hierarchic pin balls for the EUROPLEXUS software system, technical note No. 265, CCR ISPRA, Sept. 2003

[16] R.M. Mc Neal, R.L. Harder, A proposed standard set of problems to test finite element accuracy, Finite Element Analysis Design 1 (1985) 3–20

[17] T. Belytschko, P. Krysl, Analysis of thin shells by the EFG Method, Int. J. Solids Struct. 33 (2002) 3057–3080

[18] S. Potapov, B. Maurel, A. Combescure, Using SPH method to model fluid structure interaction in fast transient dynamics, Proc. ECCOMAS Thematic conference on computational methods in structural dynamics and seismic engineering, 13–16 June 2007, ed. M. Papadrakakis, D.C. Charmpis, N.D. Lagaros, Y. Tsompanakis, Rethymno, Crete, Greece